

Manipulation of Majorana Modes in a Double Quantum Dot

Jesus D. Cifuentes¹ and Luis G. G. V. Dias da Silva¹

¹*Instituto de Física, Universidade de São Paulo, C.P. 66318, 05315-970 São Paulo, SP, Brazil*
(Dated: December 18, 2018)

(To be written)

I. INTRODUCTION

In the last few decades the interest in the so called Majorana fermions has been increasing. The particle proposed by the physicist Ettore Majorana as the real field solution of the Dirac equation describes a fermion which is its own antiparticle, hence it has no charge nor mass. To the date no fundamental particle with these characteristics has been found. However, theoretical research predicts that Majorana Fermions emerge as quasi-particles at the boundary of certain topological superconductors. Kitaev¹ Recently, the new technological innovations allowed the observation of Majorana signatures in different topological materials.²⁻⁵

Despite the positive experimental results, their is still certain skepticism about the existence of Majorana Fermions. One of the reasons is that some properties of Majorana quasiparticles like the expected non-abelian statistics have not been measure. This property is of especial interest due to its promising applications in topological quantum computing. The braiding protocol based on Majorana's non-abelian statistics is the key to fault-tolerant quantum computation.^{6,7}

A promising method to detect Majorana modes consists in attaching a quantum dot (QD) to the edges of a Majorana chain in the topological phase and executing transport measurements through the QD.⁸ The Majorana mode at the end of the chain then leaks inside the QD⁹ which produces a zero-bias conductance peak of half a quanta $\frac{e^2}{2h}$ through the dot. This is a Majorana signature which produces half of the expected peak by a regular fermion. Recently, experiments including hybrid Majorana-QD systems have been performed.¹⁰ In addition, the similarity of this phenomenon with the Kondo effect, where the zero-bias conductance peak takes $\frac{e^2}{h}$, motivated the study of combined Kondo-Majorana physics in this system.^{11,12} This project revealed the existence of a region of parameters where both, Kondo and Majorana physics, coexist.

This idea has turned on new lights into the design of quantum architectures,^{13,14} because today's precise experimental control over the parameters of QDs - energy levels, tunneling couplings, etc. - offers the unique possibility of manipulating the Majorana modes inside multi-dot systems. The simplest case where Majorana manipulation is possible is in a double quantum dot. So far, no complete analysis of this simple case has been done. The goal of this project is to fill this gap by realizing a full quantum transport study of the effects of coupling

a Majorana mode with a double quantum dot. By tuning the QD gate voltages and the Majorana couplings we will be able to probe the mobility of the Majorana modes through the dots.

We considered both interacting and non-interacting cases. For interacting systems we used a obtained the exact transport description. On non-interacting models we used a NRG approach. We found that in symmetric couplings In the non-interacting case, we confirmed that shifting the QDs gate voltage induces the Majorana to tunnel only to the other dot. In addition, an indirect coupling of the second dot could cause destructive interference with the Majorana signature. In the interacting case, the NRG simulations confirmed these results and showed that other interacting effects - like Kondo and RKKY¹⁵⁻¹⁷ - could coexist with the Majorana signatures. On the other hand, when only one QD is coupled to the leads and the other Dot is attached to the QD, the Kondo effect is annihilated due to the destructive interference generated by extra dot¹⁸. Our study includes how the Majorana mode interacts with these two effects.

II. MODEL AND METHODS

We consider the setup shown in Figure 6 in which a Majorana mode at the edge of Topological Superconductor (TS) is coupled to a double quantum dot (DQD), which is attached to a single metallic lead. The Hamiltonian of this system can be partitioned in four terms: the DQD Hamiltonian H_{DQD} , the Lead Hamiltonian H_{Lead} , the DQD-lead interaction $H_{DQD-Lead}$ and the coupling between the DQD and the Majorana mode H_{M-DQDs} and

$$H = H_{DQD} + H_{Lead} + H_{DQD-Lead} + H_{M-DQDs} \quad (1)$$

The interacting Anderson Model describes the DQD-lead system

$$H_{DQD} = \sum_{i \in \{1,2\}} \sum_{\sigma \in \{\downarrow, \uparrow\}} \left(\epsilon_{di} + \frac{U_i}{2} \right) \hat{n}_{i\sigma} + \frac{U_i}{2} (\sum_{\sigma} \hat{n}_{i\sigma} - 1)^2 \\ + \sum_{\sigma \in \{\uparrow, \downarrow\}} t_{dots} (d_{1\sigma}^\dagger d_{2\sigma} + d_{2\sigma}^\dagger d_{1\sigma}), \quad (2)$$

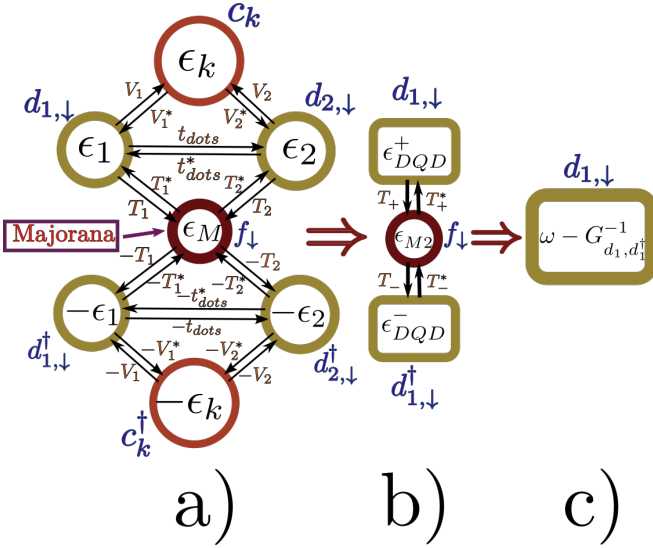


FIG. 2: Transport flow in a DQD Majorana system.

$$G_{d_{1\downarrow}, d_{1\downarrow}^\dagger}(\omega) = \frac{1}{\omega - \epsilon_{DQD}^+ - \frac{\|T_+\|^2}{\omega - \epsilon_{M2} - \frac{\|T_-\|^2}{\epsilon_{DQD}^-}}}. \quad (7)$$

The final result will depend on the broadening parameter of QD i with the lead (Γ_i). This broadening satisfies the equation

$$-i\Gamma_i = \lim_{s \rightarrow 0} \sum_k \frac{V_i^* V_i}{\omega + is - \epsilon_k}. \quad (8)$$

By convention we will take Γ_1 as the energy unit for the rest of the project. Finally we compute the DOS

$$\rho_{1\sigma}(\omega) = -\frac{1}{\pi} \text{Im} \left[G_{d_{1\sigma}, d_{1\sigma}^\dagger}(\omega) \right]. \quad (9)$$

Similar results can be obtained for the DOS of the second $\rho_{2\sigma}$. Comparing these results for both dots at the Fermi energy we will be able to determine which dot exhibits a Majorana signature.

C. Interacting case (NRG)

For the interacting case, we used the Numerical Renormalization Group (NRG) approach²¹⁻²³. The algorithm assumes a Coulomb repulsion of $U = 17.3\Gamma_1$ at both dots and a cut-off energy $D = 2U = 34.6\Gamma_1$. The spacing between the nearest energy levels is assumed to be higher than D , hence only one level is relevant in the dynamics of the system. Particle-Hole-Symmetry at each dot is obtained when $\epsilon_i = \frac{U}{2}$. At this point, there is an odd number of

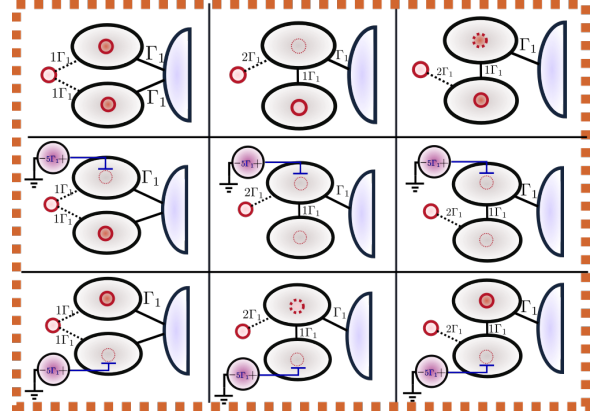


FIG. 3: Manipulation of majorana signatures according to the different connections

electrons at each dot. Hence, at sufficiently low temperature the system will exhibit the characteristic Kondo peak Wilson²¹. Observing how the Kondo-effect interacts with the Majorana signature in the double quantum dot is also an insight of this project.

To improve the efficiency of the code we took advantage of the preserved symmetries: The spin- \uparrow particle number \hat{N}_\uparrow and the spin- \downarrow parity $\hat{P}_\downarrow = \pm$ (+ even, - odd). The spin- \downarrow particle number is not preserved due to the Majorana coupling (6). The initial Hamiltonian is organized in blocks according to these symmetries. This block structure is preserved during the entire iteration process²³. To compute the spectral functions we use the density matrix renormalization group (DM-NRG) approach.²⁴

III. RESULTS

A. Non-interacting dots

In non-interacting dots ($U = 0$), the density of states at each dot can be obtained from equation (9) by replacing the Green function at (7). The manipulation of the Majorana mode is achieved by tuning the model parameters ($t_1, t_2, \epsilon_1, \epsilon_2, t_{dots}$). Fig. 3 shows 9 possible processes. The first column shows a symmetric coupling of both QDs with the lead and the Majorana mode. In columns two and three the second dot is attached indirectly to the lead through the first dot. The Majorana mode can be either attached to the first dot (column 2) or to the second dot (column 3). In the first row we assume that the gate voltage through both dots is 0 ($\epsilon_1 = \epsilon_2 = 0$), hence the density of states is particle-hole symmetric ($\rho(\omega) = \rho(-\omega)$). The Majorana signature can be manipulated by increasing the gate voltage at QD1 (second row) or QD2 (third row).

The density of states for the set-ups in column 1 (FIG. 3) is shown in Figure 4. Since the model is non-

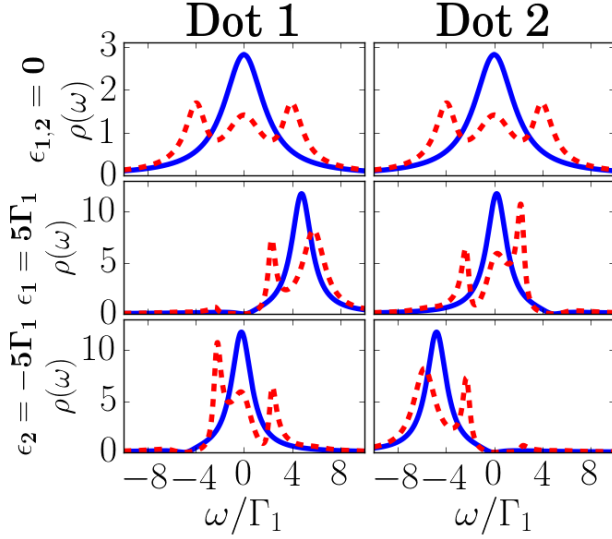


FIG. 4: Density of states in the symmetric coupling arrangement (Fig.3 first column). Solid lines: Spin-\$\uparrow\$ DOS. Dashed lines: Spin-\$\downarrow\$ DOS.

interacting, spin-\$\uparrow\$ and spin-\$\downarrow\$ models are independent. The spin-\$\downarrow\$ DOS (dashed line) shows the effects caused by the Majorana mode in comparison with the spin-\$\uparrow\$ results (solid line). In the particle hole symmetric case the DOS is equal in both dots. Note that that the spin-\$\downarrow\$ DOS is the half of the spin-\$\uparrow\$ DOS at the fermi energy $\rho_{\downarrow}(0) = \rho_{\uparrow}(0)$. This is a Majorana signature similar to the one observed in the single dot case⁸. Hence, the Majorana tunnels inside both dots. When a positive or negative gate voltage is induced in one of the dots, the Majorana mode is induced to leave that dot. As consequence the Majorana signature will only appear in the other dot.

If the second dot is not directly connected to the lead some interesting results appear. In this set-up the induced tunneling between both dots generated a path difference that destroys the central peak (See FIG5 spin-\$\uparrow\$ line). If the Majorana mode is connected to the first dot, this interference will destroy the Majorana signature in the first dot. Interestingly, it is possible to observe a clear Majorana signature in the second dot characterized by a half central peak in the spin-\$\downarrow\$ DOS. While turning on the first dot gate volge seems to destroy this Majorana signature, tuning the second dots gate voltage returns the Majorana signature to the first dot.

Instead, if the Majorana mode is attached to the second dot in the previous arrangement, then both dots will exhibit a Majorana signature. However, the signature in dot 1 is different from the others. The spin-\$\downarrow\$ DOS reveals the emergence of a zero mode with height close to 5.2 (such that $\pi\Gamma_1\rho_{\downarrow}(0) = 0.5$). This new type of Majorana signature is the result of an indirect connection between dot 1 and the Majorana mode through the sec-

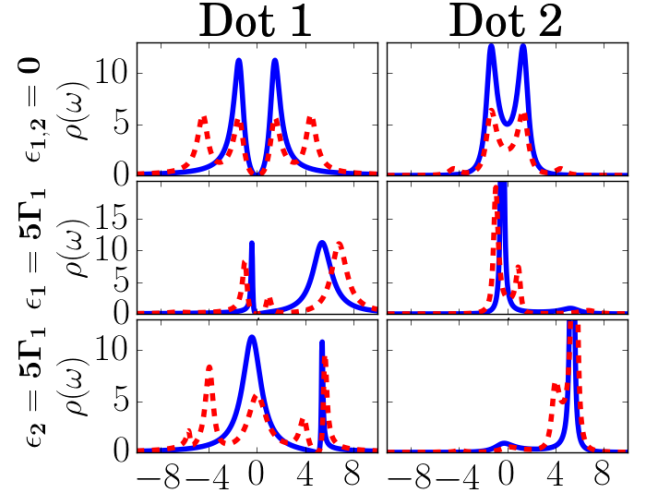


FIG. 5: Density of states in both dots of the case where the only the first QD is attached to both Majorana and Lead (Fig.3 second column) . Solid lines: Spin-\$\uparrow\$ DOS. Dashed lines: Spin-\$\downarrow\$ DOS.

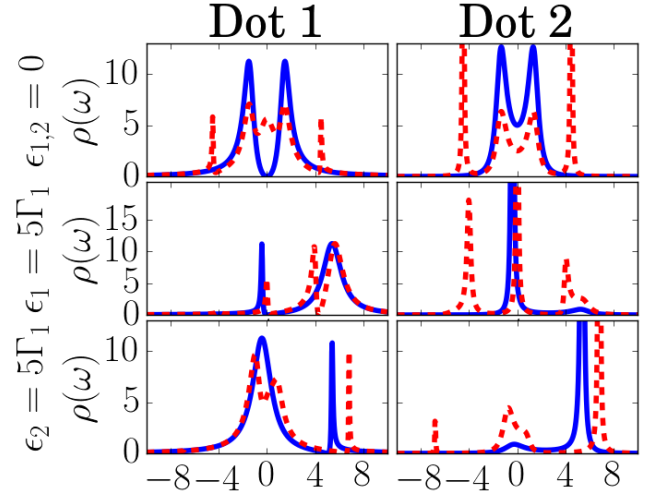


FIG. 6: Density of states of both dots in the case where only de first QD is attached to the lead and the Majorana mode is attached to the second QD. (Fig.3 third column) . Solid lines: Spin-\$\uparrow\$ DOS. Dashed lines: Spin-\$\downarrow\$ DOS.

ond dot. As in the previous case, turning on the gate voltage in dot 1 destroys the Majorana signature in both dots. However, if the gate voltage in dot 2 is turned on, the Majorana mode will leave QD2 but the indirect Majorana signature will prevail in QD1.

B. Interacting dots

Two types of majorana signatures are observed, both of them robust under a close range of parameters.

- **Type I:** The spin- \downarrow DOS is the half of the spin- \uparrow DOS at the Fermi energy ($\rho_{\downarrow}(0) = \rho_{\uparrow}(0)$).
- **Type II:** The spin- \downarrow Fermi energy is equal about 5.2. This is the value such that $\pi\Gamma_1\rho_{\downarrow}(0) = 0.5$, characteristic of a decay of half a quanta in the conductivity.

C. Manipulation in non-interacting QDs

D. Manipulation in interacting QDs

IV. CONCLUDING REMARKS

Conclusion goes here.

ACKNOWLEDGMENTS

The authors thank Edson Vernek for enlightening discussions. L.G.G.V.D.S. acknowledges financial support by CNPq (grants No. 307107/2013-2 and 449148/2014-9), and FAPESP (grant No. 2016/18495-4).

-
- ¹ A. Y. Kitaev, *Physics-Uspekhi* **44**, 131 (2001).
 - ² V. Mourik, K. Zuo, S. M. Frolov, S. R. Plissard, E. P. a. M. Bakkers, and L. P. Kouwenhoven, *Science* **336**, 1003 (2012).
 - ³ A. Das, Y. Ronen, Y. Most, Y. Oreg, M. Heiblum, and H. Shtrikman, *Nature Physics* **8**, 887 (2012).
 - ⁴ M. T. Deng, C. L. Yu, G. Y. Huang, M. Larsson, P. Caroff, and H. Q. Xu, *Nano Letters* **12**, 6414 (2012).
 - ⁵ H. Zhang, C.-X. Liu, S. Gazibegovic, D. Xu, J. A. Logan, G. Wang, N. van Loo, J. D. S. Bommer, M. W. A. de Moor, D. Car, R. L. M. Op het Veld, P. J. van Veldhoven, S. Koelling, M. A. Verheijen, M. Pendharkar, D. J. Pennachio, B. Shojaei, J. S. Lee, C. J. Palmstrm, E. P. A. M. Bakkers, S. D. Sarma, and L. P. Kouwenhoven, *Nature* **556**, 74 (2018).
 - ⁶ A. Y. Kitaev, *Annals of Physics* **303**, 2 (2003), arXiv: quant-ph/9707021.
 - ⁷ S. D. Sarma, M. Freedman, and C. Nayak, *npj Quantum Information* **1**, 15001 (2015).
 - ⁸ D. E. Liu and H. U. Baranger, *Physical Review B* **84** (2011), 10.1103/PhysRevB.84.201308, arXiv: 1107.4338.
 - ⁹ E. Vernek, P. H. Penteado, A. C. Seridonio, and J. C. Egues, *Physical Review B* **89**, 165314 (2014).
 - ¹⁰ M. T. Deng, S. Vaitiekėnas, E. B. Hansen, J. Danon, M. Leijnse, K. Flensberg, J. Nygard, P. Krogstrup, and C. M. Marcus, *Science* **354**, 1557 (2016).
 - ¹¹ M. Lee, J. S. Lim, and R. Lopez, *Physical Review B* **87**, 241402 (2013).
 - ¹² D. A. Ruiz-Tijerina, E. Vernek, L. G. G. V. Dias da Silva, and J. C. Egues, *Physical Review B* **91**, 115435 (2015).
 - ¹³ M. Barkeshli and J. D. Sau, *arXiv:1509.07135 [cond-mat, physics:quant-ph]* (2015), arXiv: 1509.07135.
 - ¹⁴ T. Karzig, C. Knapp, R. M. Lutchyn, P. Bonderson, M. B. Hastings, C. Nayak, J. Alicea, K. Flensberg, S. Plugge, Y. Oreg, C. M. Marcus, and M. H. Freedman, *Physical Review B* **95**, 235305 (2017).
 - ¹⁵ M. A. Ruderman and C. Kittel, *Physical Review* **96**, 99 (1954).
 - ¹⁶ T. Kasuya, *Progress of Theoretical Physics* **16**, 45 (1956).
 - ¹⁷ K. Yosida, *Physical Review* **106**, 893 (1957).
 - ¹⁸ L. G. G. V. Dias da Silva, N. Sandler, K. Ingersent, and S. E. Ulloa, *Physica E: Low-dimensional Systems and*

Nanostructures **40**, 1002 (2008).

- ¹⁹ D. N. Zubarev, *Soviet Physics Uspekhi* **3**, 320 (1960).
- ²⁰ D. A. Spielman, *Algorithms, Graph Theory, and Linear Equations in Laplacian Matrices*, Proceedings of the International Congress of Mathematicians (2010).
- ²¹ K. G. Wilson, *Reviews of Modern Physics* **47**, 773 (1975).
- ²² M. Sindel, *Numerical Renormalization Group studies of Quantum Impurity Models in the Strong Coupling Limit*, Text.PhDThesis, Ludwig-Maximilians-Universitt Mnchen (2005).
- ²³ R. Bulla, T. A. Costi, and T. Pruschke, *Reviews of Modern Physics* **80**, 395 (2008).
- ²⁴ W. Hofstetter, *Physical Review Letters* **85**, 1508 (2000).

Appendix A: Computation of the Green Function

In Zubarev's fermionic ballistic transport approach¹⁹ the green functions associated to two operators $A(t)$, $B(t)$ is defined as that Fourier transform of the time-ordered anti-commutator of A and B

$$G_{A,B}(\omega) = \mathcal{F}\{\mathcal{T}[[A(t), B(t')]]\}(\omega). \quad (\text{A1})$$

The Fourier transform of Schrodinger evolution determines the transport equations

$$\omega G_{A,B}(\omega) = \delta_{A^{\dagger},B} + G_{[A,H],B}(\omega). \quad (\text{A2})$$

We can apply this to Hamiltonian (1) by replacing A and B by the creation and annihilation operators. To simplify the complexity of the system we fix $B = d_{1\downarrow}^{\dagger}$. In addition note that the transport equations for f_{\downarrow} and f_{\downarrow}^{\dagger} are

$$(\omega - \epsilon_M) G_{f_{\downarrow}, d_{1\downarrow}^{\dagger}}(\omega) = \frac{t}{\sqrt{2}} \left(G_{d_{1\downarrow}, d_{1\downarrow}^{\dagger}}(\omega) - G_{d_{1\downarrow}^{\dagger}, d_{1\downarrow}^{\dagger}}(\omega) \right) \quad (\text{A3})$$

$$(\omega + \epsilon_M) G_{f_{\downarrow}^{\dagger}, d_{1\downarrow}^{\dagger}}(\omega) = \frac{t}{\sqrt{2}} \left(G_{d_{1\downarrow}, d_{1\downarrow}^{\dagger}}(\omega) - G_{d_{1\downarrow}^{\dagger}, d_{1\downarrow}^{\dagger}}(\omega) \right), \quad (\text{A4})$$

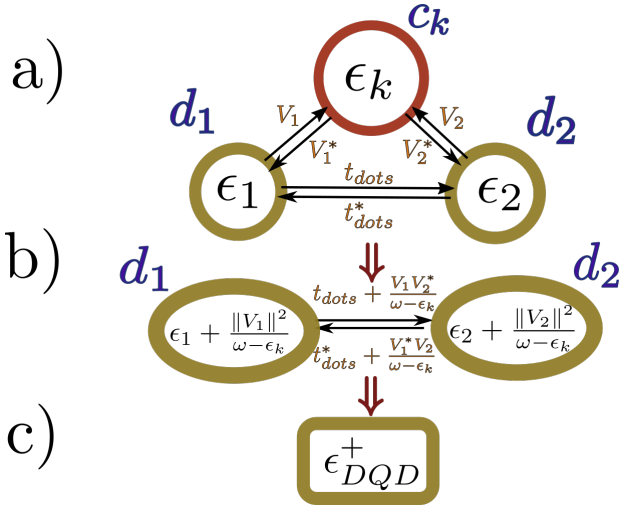


FIG. 7

which allows us to take $G_{f_{\downarrow}, d_{1\downarrow}}^{\dagger}(\omega) = \frac{\omega + \epsilon}{\omega - \epsilon} G_{f_{\downarrow}, d_{1\downarrow}}^{\dagger}(\omega)$. Therefore, we can eliminate $G_{f_{\downarrow}, d_{1\downarrow}}^{\dagger}(\omega)$ from the equations even before we start Gauss-Jordan process.

Writing the other equations we obtain the linear system

$$T \vec{G}_{d_1^{\dagger}} = \hat{e}_1 \quad (\text{A5})$$

where T is the transport matrix

$$\begin{bmatrix} \omega - \epsilon_1 & -V_1^* & -t_{dots} & \frac{-t_1}{\sqrt{2}} & 0 & 0 & 0 \\ -V_1 & \omega - \epsilon_k & -V_2 & 0 & 0 & 0 & 0 \\ -t_{dots}^* & -V_2^* & \omega - \epsilon_2 & \frac{-t_2}{\sqrt{2}} & 0 & 0 & 0 \\ \frac{-\sqrt{2}t_1^*}{\omega + \epsilon_M} & 0 & \frac{-\sqrt{2}t_2^*}{\omega + \epsilon_M} & \omega - \epsilon_M & \frac{\sqrt{2}t_2^*}{\omega + \epsilon_M} & 0 & \frac{\sqrt{2}t_1^*}{\omega + \epsilon_M} \\ 0 & 0 & 0 & \frac{t_2}{\sqrt{2}} & \omega + \epsilon_2 & V_2^* & t_{dots}^* \\ 0 & 0 & 0 & 0 & V_2 & \omega + \epsilon_k & V_1 \\ 0 & 0 & 0 & \frac{t_1}{\sqrt{2}} & t_{dots} & V_1^* & \omega + \epsilon_1 \end{bmatrix}, \quad (\text{A6})$$

$\vec{G}_{d_1^{\dagger}}$ is the column vector

$$[G_{d_{1\downarrow}, d_{1\downarrow}}^{\dagger}(\omega), G_{c_{k\downarrow}, d_{1\downarrow}}^{\dagger}(\omega), G_{d_{2\downarrow}, d_{1\downarrow}}^{\dagger}(\omega), G_{f_{\downarrow}, d_{1\downarrow}}^{\dagger}(\omega), G_{d_{2\downarrow}, d_{1\downarrow}}^{\dagger}(\omega), G_{c_{k\downarrow}, d_{1\downarrow}}^{\dagger}(\omega), G_{d_{1\downarrow}, d_{1\downarrow}}^{\dagger}(\omega)]^T$$

and \hat{e}_1 is the vector with entries $\hat{e}_{1_n} = \delta_{1n}$.

The graph associated to this matrix is the one in FIG. 7.a). The energies inside each vertex are given by subtracting the corresponding diagonal term from ω . The couplings are just the negative of the off-diagonal terms.

1. The double quantum dot

To explain the process of Gaussian elimination we will obtain the green function for the case without Majorana

fermion ($t_1 = t_2 = 0$). The transport matrix for this system is

$$\begin{bmatrix} \omega - \epsilon_1 & -V_1 & -t_{dots} \\ -V_1^* & \omega - \epsilon_k & -V_2 \\ -t_{dots}^* & -V_2^* & \omega - \epsilon_2 \end{bmatrix}. \quad (\text{A7})$$

The graph associated to this matrix can be observed in FIG. 7.a). To eliminate the vertex c_k we just need to subtract from (A7) the rank-1 matrix that cancels the row and the column corresponding to c_k . This matrix is

$$\begin{bmatrix} \frac{V_1^* V_1}{\omega - \epsilon_k} & -V_1^* & \frac{V_2 V_1^*}{\omega - \epsilon_k} \\ -V_1 & \omega - \epsilon_k & -V_2 \\ \frac{V_2^* V_1}{\omega - \epsilon_k} & -V_2^* & \frac{V_2^* V_2}{\omega - \epsilon_k} \end{bmatrix}. \quad (\text{A8})$$

The result of (A7) - (A8) is

$$\begin{bmatrix} \omega - \epsilon_1 - \frac{V_1^* V_1}{\omega - \epsilon_k} & 0 & -t_{dots} - \frac{V_2 V_1^*}{\omega - \epsilon_k} \\ 0 & 0 & 0 \\ -t_{dots}^* - \frac{V_2^* V_1}{\omega - \epsilon_k} & 0 & \omega - \epsilon_2 - \frac{V_2^* V_2}{\omega - \epsilon_k} \end{bmatrix} \quad (\text{A9})$$

which is depicted by the graphs in FIG. 7.b). The next step is to pop-out the vertex d_2 following the same procedure. At the end, the energy inside the vertex d_1 will be

$$\epsilon_{DQD}^+ = \epsilon_1 + \sum_{\mathbf{k}} \frac{V_1 V_1^*}{\omega - \epsilon_{\mathbf{k}}} + \frac{\left\| t_{dots} + \sum_{\mathbf{k}} \frac{V_1 V_2^*}{\omega - \epsilon_{\mathbf{k}}} \right\|^2}{\omega - \epsilon_2 - \sum_{\mathbf{k}} \frac{V_2^* V_2}{\omega - \epsilon_{\mathbf{k}}}} \quad (\text{A10})$$

and the green function of $G_{d_1 d_1^{\dagger}}(\omega)$ in a DQD will be given by $\frac{1}{\omega - \epsilon_{DQD}}$ (see FIG. 7.c)).

2. Solution of the transport equations

The previous procedure can be generalized into the following algorithm:

1. Computing the transport equations with the second term fixed in the creation operator of the dot.
2. Setting up the graph associated to the transport system.
3. Popping out the vertexes of the graph. Each popping process carries the following steps.
 - (a) Computing the extra-terms in the energies and couplings based on the walks passing through the popped vertex.
 - (b) Eliminating this vertex from the graph.
 - (c) Iterating till there is only one vertex.
4. The energy in the remaining vertex d is $\epsilon_d = \frac{1}{\omega - G_{d, d^{\dagger}}(\omega)}$.

Following these steps it is possible to solve the general case. We start with the graph in FIG.2 and we pop out the vertexes $c_k, c_k^\dagger, d_{2,\downarrow}$ and $d_{2,\downarrow}^\dagger$ in that order. The energies associated to $d_{1,\downarrow}$ and $d_{1,\downarrow}^\dagger$ will be similar to (A10) giving

$$\epsilon_{DQD}^\pm = \pm\epsilon_1 + \sum_{\mathbf{k}} \frac{V_1 V_1^*}{\omega - \epsilon_{\mathbf{k}}} + \frac{\left\| \pm t_{dots} + \sum_{\mathbf{k}} \frac{V_1 V_2^*}{\omega - \epsilon_{\mathbf{k}}} \right\|^2}{\omega \pm \epsilon_2 - \sum_{\mathbf{k}} \frac{V_2 V_2^*}{\omega - \epsilon_{\mathbf{k}}}}. \quad (\text{A11})$$

There is also a correction in the couplings between the Majorana mode and $d_{1,\downarrow}, d_{1,\downarrow}^\dagger$ given by

$$T_\pm = \pm t_1 \pm t_2 \frac{\left(\pm t_{dots} + \sum_{\mathbf{k}} \frac{V_1 V_2^*}{\omega - \epsilon_{\mathbf{k}}} \right)}{\omega \pm \epsilon_2 \pm \sum_{\mathbf{k}} \frac{V_2 V_2^*}{\omega - \epsilon_{\mathbf{k}}}}. \quad (\text{A12})$$

Finally since the Majorana is in contact with dot 2, there is an extra-term appearing in the Majorana energy given by

$$\epsilon_{M2} = \omega - \epsilon_M - \frac{\frac{\omega}{\omega + \epsilon_M} \|t_2\|^2}{\omega - \epsilon_2 - \sum_{\mathbf{k}} \frac{V_2 V_2^*}{\omega - \epsilon_{\mathbf{k}}}} - \frac{\frac{\omega}{\omega + \epsilon_M} \|t_2\|^2}{\omega + \epsilon_2 - \sum_{\mathbf{k}} \frac{V_2 V_2^*}{\omega + \epsilon_{\mathbf{k}}}}. \quad (\text{A13})$$

With all the terms of the graph in FIG.2.b) computed, it only remains to pop out vertexes d_1^\dagger and f_\downarrow in that order to obtain the green function in equation (7).